Revision 2

Expanding the speciation of terrestrial molybdenum: discovery of polekhovskyite, $MoNiP_2$, and insights into the sources of Mo-phosphides in the Dead Sea Transform area

Sergey N. Britvin[1,2]*, Mikhail N. Murashko[1], Oleg S. Vereshchagin[1], Yevgeny Vapnik[3], Vladimir V. Shilovskikh[4], Natalia S. Vlasenko[4], and Vitalii V. Permyakov[5]

[1] Institute of Earth Sciences, St. Petersburg State University, Universitetskaya Nab. 7/9, 199034 St. Petersburg, Russia

[2] Kola Science Center, Russian Academy of Sciences, Fersman Str. 14, 184200 Apatity, Russia

[3] Department of Geological and Environmental Sciences, Ben-Gurion University of the Negev, P.O.B. 653, Beer-Sheva 84105, Israel

[4] Centre for Geo-Environmental Research and Modeling, St. Petersburg State University, Ulyanovskaya ul. 1, 198504 St. Petersburg, Russia

[5] Institute of Geological Sciences, National Academy of Sciences of Ukraine, Gontchara Str., 55b, Kiev 01054, Ukraine

Abstract

Polekhovskyite, $MoNiP_2$, is the first terrestrial Mo phosphide, a phosphorus-rich homologue of meteoritic monipite, MoNiP. The mineral represents a novel, phosphide type of terrestrial Mo speciation. It was discovered among phosphide assemblages in pyrometamorphic rocks of the Hatrurim Formation (the Mottled Zone) in Israel, the area confined to the Dead Sea Transform fault system. Polekhovskyite occurs in the altered diopside microbreccia, as micrometer-sized euhedral crystals intimately intergrown with murashkoite, FeP, and transjordanite, Ni_2P, in association with Si-rich fluorapatite, hematite and magnetite. In reflected light, the mineral has a bluish-grey colour with no observable bireflectance and anisotropy. Chemical composition (electron microprobe, wt.%): Mo 44.10, Ni 22.73, Fe 4.60, P 29.02, total 100.45, that corresponds to the empirical formula $Mo_{0.99}(Ni_{0.83}Fe_{0.18})_{1.01}P_{2.01}$ and leads to the calculated density of 6.626 g cm^{-1}. Polekhovskyite is hexagonal, space group $P6_3/mmc$, a 3.330(1), c 11.227(4) Å, V 107.82(8) $Å^3$, and $Z = 2$. The crystal structure has been solved and refined to $R_1 = 0.0431$ based on 50 unique observed reflections. The occurrence of Mo-bearing phosphides at the Dead Sea Transform area is a regional-scale phenomenon, with the localities tracked across both Israel and Jordan sides of the Dead Sea. The possible sources of Mo required for the formation of Mo-bearing phosphides are herein reviewed; they are likely related to the processes of formation of the Dead Sea Transform fault system. The problem of anthropogenic contamination of geological samples with Mo and Ni is also discussed in the paper, in context of the general aspects of discrimination between natural and technogenic ultra-reduced phases.

Keywords: molybdenum, phosphide, pyrometamorphism, meteorite, carbonaceous chondrite, Ca-Al-rich inclusions, Dead Sea Rift, anthropogenic contamination

Introduction

Molybdenum, as an element, is a sensitive geochemical marker whose redox and isotopic speciation allows tracing diverse planetary processes (Kendall et al. 2017; Greaney et al. 2018). The dominant Mo mineral in the lithosphere is its sulfide, molybdenite MoS_2, which crystallizes in systems where the nearest relative of Mo, tungsten, appears in the form of tungstate anions, $(WO_4)^{2-}$ (Smedley and Kinniburgh 2017). It is noteworthy that the rich family of oxygen-bearing Mo minerals (more than 60 species) owes its diversity to the secondary oxidation of molybdenite, usually under aquatic environments (Greaney et al. 2018). The rare exceptions not related to molybdenite are confined to volcanic exhalations (Pekov et al. 2020), where pre-sublimation speciation of Mo is obscure. Thiomolybdates – the anions intermediate between $(MoO_4)^{2-}$ and $(MoS_4)^{2-}$ – are believed to play an important role in the aquatic behaviour of Mo (Erickson and Helz 2000). However, until now, thiomolybdates were not recognized as mineral species in the solid state. Altogether, the fate of Mo in the lithosphere can be expressed as a redox-dependent cycling between its sulfide and oxide forms (Erickson and Helz 2000; Greaney et al. 2018). In meteorites, molybdenite was for a long time the sole known Mo mineral (Fuchs and Blander 1977; Armstrong et al. 1987). It is a rare constituent of specific assemblages called Fremdlinge (El Goresy et al. 1978). The latter represent the opaque, μm- to mm-sized droplets consisting of Fe-Ni metal, sulfides with inclusions of refractory metal alloys, oxides, silicates and phosphates (El Goresy et al. 1978). Fremdlinge occur in CV3 carbonaceous chondrites, where they are found within calcium-aluminium rich inclusions (CAI) - the oldest known objects in the Solar System (Amelin et al. 2010). Recent investigations revealed that Fremdlinge may bear a diverse suite of Mo-minerals not limited to sulfides and oxides, including the first natural Mo-phosphide, monipite MoNiP (Ma et al. 2014).

In the course of ongoing research of phosphide assemblages of the Hatrurim Formation in Israel and West Jordan, the substantial enrichment in Mo was revealed among phosphides described in this area (Britvin et al. 2020a, 2021b). Phosphide speciation of Mo is quite unusual for Earth, as

emphasized by the present discovery of the first known terrestrial Mo-phosphide, $MoNiP_2$ which is, from the chemical point of view, is a higher phosphide homologue of meteoritic mineral monipite, MoNiP (Ma et al. 2014). We herein present the description of this mineral, named polekhovskyite in honour of Yury Stepanovich Polekhovsky (1947–2018), Russian geologist and mineralogist, for his contributions to the studies of opaque minerals, including phosphides (Britvin et al. 2015; 2019a,b; 2020a,b). Both the mineral and its name have been approved by the Commission on New Minerals, Nomenclature and Classification, International Mineralogical Association (2018-147). The holotype specimen of polekhovskyite is deposited in the collections of the Fersman Mineralogical Museum of the Russian Academy of Sciences, Moscow, Russia, with the registration number 5287/1. Besides the report on a new mineral, the sources of Mo in phosphides of the Mottled Zone are herein discussed, which were likely linked to the onset of activity at the Dead Sea Transform fault system. Last but not least, the present article touches on the persistent problem of anthropogenic contamination of heavy mineral concentrates with Ni and Mo, following the discussions raised in the recent works by Litasov et al. (2019, 2020) and Ballhaus et al. (2021).

The Hatrurim Formation

This rock complex is located in the Levant region of the Middle East (Britvin et al. 2021a) (Fig. 1). The term "Hatrurim Formation" was originally introduced to describe a suite of metamorphosed sediments constituting the Hatrurim Basin – a hilly terrain that occupies an area of about 50 km^2 in the vicinity of the Dead Sea, ca. 15 km northwest of Mount Sedom (Gross 1977) (Fig. 1). Another common name for this suite, "the Mottled Zone" (Picard 1931), emphasizes the unusual coloration and patchy structures of its diverse metamorphic lithologies. Today, the names "Hatrurim Formation" and "the Mottled Zone" are often used in a broader sense – to refer to the world's largest suite of pyrometamorphic rocks whose outcrops are exposed over an area of 150×200 km around the Dead Sea Transform (traced by the Jordan valley), encompassing central to

north Israel, West Bank and central to west Jordan (Fig. 1) (e.g., Burg et al. 1992; Vapnik et al. 2007; Novikov et al. 2013).

The rugged terrain of the Hatrurim Basin in the Negev desert, Israel, is composed of numerous hills up to 80 m in relief, dissected by a system of dry wadi – tributaries to the Dead Sea (e.g., Britvin 2021b). The lack of vegetation and quaternary cover (Fig. 2a, 2c) affords favorable conditions for the sampling of metamorphic rocks. The latter appear as cliffs and lenses composed of diverse lithologies produced by combustion metamorphism (pyrometamorphism) – a process involving high-temperature and low-pressure calcination and fusion of the sediments (e.g., Vapnik et al. 2015). The conditions of metamorphism corresponded to sanidinite facies; the local temperatures might reach 1200–1450 °C at near-atmospheric pressure (Sharygin et al. 2016). The main types of pyrometamorphic rocks are spurrite, gehlenite, larnite marbles, and anorthite–pyroxene hornfelses (Gross 1977). The fused rocks, called paralavas (Vapnik et al. 2007), are less common. The total preserved thickness of metamorphic complex is about 100 m (Fig. 3). The stratigraphic equivalent of the Mottled Zone in Israel is the Ghareb and Taqiye chalky–marly sequence of Maastrichtian to Paleocene age (Gross 1977) (Fig. 3). The upper contacts of phosphorites of the Mishash Formation (Campanian age) underlying the Mottled Zone (Fig. 3) are sporadically affected to pyrometamorphic alteration.

The largest pyrometamorphic massif of the Hatrurim Formation is the Daba-Siwaqa complex, which occupies 330 km^2 of the Transjordan Plateau, 25–80 km south of Amman, Jordan (Fig. 1). The metamorphic rocks of Daba-Siwaqa appear as a chain of 30-80 m high hills on the plateau composed of Maastrichtian–Danian bituminous chalk, Paleocene limestone (Muwaqqar Formation) and Eocene chert and limestone (Umm Rijam Formation) (Novikov et al. 2013; Al-Tawalbeh et al. 2017) The total preserved thickness reaches 200 m (Fig. 3). Pyrometamorphic rocks are represented by spurrite and fluorapatite marbles with a few occurrences of larnite marbles. Paralavas were revealed at one locality.

Pyrometamorphic lithologies of the Mottled Zone, both in Israel and Jordan, were subjected to pronounced hydrothermal alteration and weathering (Gross 1977; Burg et al. 1992; Khoury 2020). Altogether, superposition of various processes has resulted in an unprecedented mineral diversity (more than 240 species), ranging from reduced associations of phosphides and Ca-sulfides (Britvin et al. 2015; Galuskina et al. 2017) to extremely oxidized assemblages containing chromate(VI) and selenate(VI) ions, $(CrO_4)^{2-}$ and $(SeO_4)^{2-}$ (Juroszek et al. 2020).

According to K–Ar and $^{40}Ar/^{39}Ar$ dating of pyrometamorphic rocks of the Hatrurim Basin, the major metamorphic events at the Mottled Zone might occur in Miocene (16 Ma) and Pliocene-Pleistocene (4.0–1.5 Ma), although age determinations of 200 Ka were also reported (Burg et al. 1992; Gur et al. 1995 and the references cited therein). The Miocene event chronologically coincides with the separation of Israel from the Arabian Plate by the Dead Sea Transform fault (Ben-Avraham et al. 2008). Although the Mottled Zone was studied since the beginning of the last century (Picard 1931), the origin of this rock complex is still a matter of debates. The most popular hypotheses include the spontaneous combustion of dispersed organic matter in the chalky–marly sequence of the Maastrichtian and Paleocene age (Gross 1977) or oil-gas (methane) firing induced by mud volcanism (Novikov et al. 2013). The recent mineralogical records evidence for possible high-pressure processes that could take place in this region, where the pressures could reach 25 GPa (Britvin 2021b, 2022). This might open new insights into the primary event(s), such as large-scale earth-meteoroid collision, which could be responsible for the initiation of combustion processes in the Mottled Zone.

Phosphides of the Mottled Zone

Phosphides are the principal carriers of reduced phosphorus in the solar system, but until the findings in the Hatrurim Formation, these minerals were practically unknown on Earth (Britvin et al. 2021c). Since the first report on phosphide occurrences in the Mottled Zone (Britvin et al. 2015),

these minerals were recognized at three localities on both sides of the Dead Sea (Fig. 1): in natural outcrops at wadi Halamish and wadi Zohar in the southern part of the Hatrurim Basin, Israel (Britvin et al. 2015; Galuskin et al. 2020) (Fig. 2a, 2c) and in the phosphorite quarry which exposes pyrometamorphic rocks of the Daba-Siwaqa complex in Jordan (Britvin et al. 2015) (Fig. 2e). In the Hatrurim Basin, phosphide-bearing lithologies were primarily found in several detrital blocks, and subsequently revealed in a ~2×2 m bedrock outcrop (Fig. 2a and 2c). In Jordan, phosphide assemblages can be found in the quarry highwalls and in the detached meter-sized rock blocks (Fig. 2e). In wadi Halamish (Israel) and Daba-Siwaqa quarry (Jordan), phosphides are confined to diopside-dominant rocks - paralavas and microbreccias (the latter likely represent hydrothermally altered paralavas) (Fig. 2b and 2f). Chemical and mineral composition of these rocks was previously reviewed by Britvin et al. (2019b). In wadi Zohar (Israel), phosphide assemblages were found in gehlenite rocks – microbreccias and paralavas described by Galuskin et al. (2020) and Britvin et al. (2022) (Fig. 2d). In all reported localities, mineral assemblages are often much enriched in phosphides, whose nests, resembling sulfides in appearance, can reach 1 cm in size (Fig. 4). In total, nine phosphide species belonging to the system Fe-Ni-P were discovered, among those six minerals are new in nature (Britvin et al. 2020c). Molybdenum phosphides are represented by polekhovskyite, $MoNiP_2$ described herein, nickolayite FeMoP (Murashko et al. 2019) and orishchinite, $(Ni,Fe,Mo)_2P$ (Britvin et al. 2019c), which are rare but were found on both sides of the Dead Sea – in Israel (polekhovskyite) and in Jordan (nickolayite and orishchinite). Subordinate contents of Mo (up to 3 wt.%) are typical in the most common phosphides belonging to the transjordanite-barringerite series, Ni_2P-Fe_2P, both in Israel and Jordan (Britvin et al. 2020a, 2021b).

Phosphide assemblages, once formed, were affected by a subsequent high-temperature alteration – oxidative pyrolysis, which resulted in the formation of specific phosphate minerals, such as pyrophosphates and cyclophosphates, with further oxidation to hematite (Britvin et al. 2021a). The geochemical processes which could lead to the emergence of phosphides in the Hatrurim

Formation were discussed by Britvin et al. (2015, 2021a). The suggested pathways are focused on the co-reduction of phosphates with Fe and Ni oxides. Phosphates could be represented by fluorapatite, $Ca_5(PO_4)_3F$, which is ubiquitous in the Mottled Zone (Gross 1977), and less common keplerite, $Ca_9(Ca_{0.5}\square_{0.5})Mg(PO_4)_7$ (Britvin et al. 2021d). The oxide concentrators of Ni are trevorite, $NiFe_2O_4$, and bunsenite, NiO (Britvin et al. 2015; Sokol et al. 2020). The formation of phosphides *via* phosphate reduction by dihydrogen, carbon or methane was well explored in synthetic chemistry and metallurgy (Lazoryak et al. 2003; Voncken et al. 2006; Burns et al. 2007). The lowermost thermal limits required for the initiation and maintenance of reduction processes (550–750 °C) agree with the formation temperatures of natural phosphides, which were below 850–900 °C (Britvin et al. 2020b, 2021b). Based on the current hypotheses on the genesis of the Mottled Zone (Gross 1977; Novikov et al. 2013), one can suggest that either dispersed bitumen or natural methane could serve as reducing agents. The recent discovery of encapsulated molecular dihydrogen in phosphide-bearing assemblages of wadi Zohar (Galuskin et al. 2020) (Fig. 2c) suggests that native dihydrogen could also play a role of reductant. Consideration of lightning strikes (Pasek and Block 2009) as reduction drivers can not be ruled out (Britvin et al. 2015), although the confinement of phosphide mineralization to the deep zones of metamorphosed strata (e.g., in the Jordan quarry) makes this hypothesis less realistic.

Analytical methods

The rock piece containing phosphide assemblages was cut into a few slices, which were polished and coated with carbon film. It should be emphasized that none of the phosphide-bearing samples was affected to any mechanical grinding or crushing – all phosphide grains were found *in-situ* in the polished sections. The thick section containing polekhovskyite was first examined under scanning electron microscope (Hitachi S-3400N) and chemically characterized using an Oxford Instruments AzTec Energy X-Max 20 EDX spectrometer at 10 kV acceleration voltage and 0.2 nA

beam current. The metal analytical standards were used to measure Fe, Ni, Co (*K*α-series) and Mo (*L*α), whereas P was measured against InP standard (P*K*α). The absence of S and Co was further confirmed qualitatively using an INCA WAVE 500 WDX spectrometer (20 kV, 15 nA). After removal of carbon coating, phosphide assemblages were examined in reflected light under optical microscope. A grain containing the biggest polekhovskyite crystals was manually removed from the section and was subjected to X-ray single-crystal study. Because of the small size of polekhovskite crystals (2 to 3 μm, Fig. 5), we did not attempt to extract a single crystal of the mineral. Instead, the whole phosphide assemblage (murashkoite with the embedded polekhovskite crystals) was used for data collection. A hemisphere of reciprocal space was collected by means of a Bruker Kappa APEX DUO CCD diffractometer using Mo*K*α radiation (frame width 0.5°; exposure time 360 s per frame). Subsequent data processing was performed using CrysAlisPro v.171.41 program package (Rigaku Oxford Diffraction). The CrysAlisPro software allows extracting and independent refinement of up to 8 orientation (UB) matrices related to separate single crystal domains. In our case, one could recognize 1 UB matrix related to the host murashkoite crystal and 4 randomly oriented UB matrices of $MoNiP_2$. Subsequent integration of each of the four $MoNiP_2$ matrices allowed selection of the best integrable domain, which was used for structure solution and refinement. The crystal structure of polekhovskite has been solved by the dual space method and refined to $R_1 = 0.0431$ using a *SHELX*-2018 set of programs (Sheldrick 2015), via an Olex2 v.1.2.8 graphical user interface (Dolomanov et al. 2009). The details of data collection, integration procedures and structure refinement can be retrieved from the crystallographic information file (CIF) included into Supplementary data. Powder X-ray diffraction pattern of polekhovskyite was calculated with Stoe WinXPOW software (Stoe and Cie GmbH).

Occurrence, appearance and chemical composition

Polekhovskite was found in phosphide-bearing rocks collected at the Nahal Halamish – a wadi passing approximately in longitudinal direction through the southern part of the Hatrurim Basin, Negev desert, Israel (Britvin et al. 2015) (Fig. 1, 2a). Phosphide assemblages are confined to severely altered diopside microbreccias enriched in hematite and magnetite (Fig. 2b). Thaumasite, tobermorite and a suite of other, poorly defined Ca- and Mg-Fe hydrous secondary silicates serves as a binder for diopside crystals. A complete list of rock-forming minerals and their compositions was reported by Britvin et al. (2019b). Si-Fe-bearing fluorapatite, $(Ca_{4.37}Fe^{2+}_{0.16})_{4.48}(P_{2.88}Si_{0.16})_{3.04}O_{11.49}F_{1.02}$, commonly occurs in the same association (Fig 5a). Polekhovskyite appears as euhedral crystals up to 3 μm in size intimately intergrown with murashkoite (FeP) or rimming transjordanite grains (Ni_2P) (Fig. 5). It has a bluish-grey colour in reflected light (Fig. 5b), with no observable bireflectance and anisotropy. Reflectance and microhardness could not be measured because of the small crystal size. Chemical composition of the mineral is given in Table 1. Taking into account the results of structure refinement, the empirical formula can be written as $Mo_{0.99}(Ni_{0.83}Fe_{0.18})_{1.01}P_{2.01}$ (based on 4 atoms per formula unit), corresponding to the ideal one $MoNiP_2$. The density calculated from the empirical formula and unit-cell parameters is 6.626 g cm^{-1}. From the chemical point of view, polekhovskyite can be regarded a higher phosphide homologue of meteoritic monipite, MoNiP (Ma et al. 2014).

X-ray powder diffraction and crystal structure

The insufficient amount of polekhovskyite precluded obtaining X-ray powder diffraction data. However, its calculated powder pattern conforms to synthetic $MoNiP_2$ (Guérin 1976) (Table 2). Taking into account that natural polekhovskite has a mixed (Ni,Fe) site population, its unit-cell parameters can be regarded as identical to the parameters of synthetic $MoNiP_2$ (Table 3). The crystal structure of polekhovskyite belongs to its own, $MoNiP_2$ structure type (Guérin et al. 1975; Guérin and Sergent 1976). The structural framework is built up of the two kinds of [MP_6] polyhedra (Fig.

6a), whose population refinement revealed the perfect ordering between Mo and (Ni,Fe). Molybdenum incorporates into trigonal prisms [MoP_6] [d(Mo–P) = 2.462(4) Å], whereas Ni and Fe populate [(Ni,Fe)P_6] octahedra [d(M–P) = 2.304(3) Å] (Fig. 6a). The coordination numbers of Mo and (Ni,Fe) in polekhovskyite are higher than those in synthetic analogue of monipite (Guérin and Sergent 1977) (Fig. 6b) – a structural consequence of the lower metal-to-phosphorus ratio in $MoNiP_2$ (1:1) relative to MoNiP (2:1).

Polekhovskyite, $MoNiP_2$, *vs.* monipite, MoNiP: formation factors

A lack of sufficient knowledge of the phase relations in the Mo–Ni–P system (Oryshchyn et al. 2001) allows only rough assessment of the conditions that governed the formation of polekhovskyite, $MoNiP_2$ instead of its nearest chemical relative, monipite, MoNiP. The synthesis of both phosphides is accomplished under the same oxygen-free environment, in the solid state at 800-1200 °C (Guérin and Sergent 1976, 1977). Therefore, the factor which likely determined the emergence of a certain phosphide is a metal-to-phosphorus ratio: crystallization of polekhovskyite apparently proceeded at higher phosphorus potential than crystallization of monipite. The deficiency of phosphorus during monipite formation is supported by the presence of (Ru,Mo,Ni) alloy and awaruite in the same Fremdling (Ma et al. 2014). In contrast, polekhovskyite assemblages do not contain metal alloys, but include murashkoite that has the same M:P atomic ratio equal to 1 (M = Fe, Ni, Mo). The morphological relationships between phosphides evidence that polekhovskyite was formed after transjordanite but prior to murashkoite, according to the sequence: Ni_2P (M:P = 2) → $MoNiP_2$ (M:P = 1) → FeP (M:P = 1). Therefore, one can assume that polekhovskyite crystallization was realized due to the excess of phosphorus not accommodated by already crystallized Ni_2P (transjordanite). In this respect, one should emphasize the extreme level of Mo fractionation between these phosphides. Transjordanite contains less than 1.4 wt.% Mo, in contrast to 44 wt.% in polekhovskyite (Table 1). However, it was shown that transjordanite is capable of incorporating

more than 3 wt.% Mo (Britvin et al. 2020a), by substitution of five-coordinated Ni towards isostructural monipite: $Ni^{IV}Ni^{V}P$ (transjordanite) → $Ni^{IV}Mo^{V}P$ (monipite). Therefore, transjordanite in the given assemblages is undersaturated with respect to Mo. Consequently, it can be inferred that the growth of polekhovskyite proceeded under unequilibrated conditions: it was either very fast or was accomplished at low temperature precluding interphase Mo diffusion.

Some insights into the origin of Mo phosphides in the Mottled Zone

The available data suggest that the enrichment of phosphide assemblages in Mo is a regional-scale phenomenon, which encompasses the localities separated by a distance of ~100 km, on both Israel and Jordan sides of the Dead Sea (Britvin et al. 2020a, 2021b) (Fig. 1). Molybdenum contents up to 3 wt.% are commonly detected in the minerals related to the join barringerite-transjordanite – hexagonal Fe_2P-Ni_2P (Britvin et al. 2020a), and in allabogdanite – the high-pressure modification of $(Fe,Ni)_2P$ (Britvin et al. 2021b). Other associated phosphides related to the Fe-Ni-P system do not contain Mo in the amounts detectable by EMPA, but sometimes exhibit the presence of thin molybdenite lamellae (Fig. 7a, 7b). In addition, powellite, $CaMoO_4$, is common in the same associations (Fleurance et al. 2013; Khoury 2020) (Fig. 7c). In view of a relatively diverse Mo mineralisation, it looks surprising that in total, pyrometamorphic lithologies of the Hatrurim Basin (Israel) are depleted in this element, showing no more than 4 ppm Mo (Bogoch et al. 1999). Therefore, it can be concluded that Mo tends to selectively concentrate within phosphide phases and powellite.

In Jordan, sedimentary sequences stratigraphically juxtaposed to the Mottled Zone are enriched in polymetallic mineralization, where Mo content may reach 950 ppm (Fleurance et al. 2013). The data available for phosphorites of the Mishash Formation in Israel, which underlies the Mottled Zone, show Mo contents of 8 to 70 ppm (Nathan et al. 1979), whereas chalks and marls of the Ghareb Formation contain up to 30 ppm Mo (Geller et al. 2012). However, there are the spatially

293 occurring lithologies on the Israel side of the Dead Sea which exhibit extreme enrichment in Mo.
294 Contents of this element up to 1000 ppm were first determined in the dolomite-chert breccia body
295 outcropping near the Arad town (Issar et al. 1969). Further prospecting has revealed a series of
296 similar outcrops of ferriginous dolomite-chert breccias, tracked in NW direction across the
297 northeastern Negev desert. The breccia bodies, being exposed on the areas from a few to several
298 dozens of square meters (Fig. 8a), are hosted by the chalky limestones, dolomites and chalks of the
299 Bina and Menuha Formations, both of Late Cretaceous age (Magaritz et al. 1983; Ilani et al. 1985)
300 (Fig. 3). The breccias are composed of irregular dolomite blocks up to 30-40 cm in size and chert
301 fragments cemented by a mixture of finely dispersed hematite and goethite, along with calcite and
302 barite (Fig. 8b). Molybdenum anomalies are confined to the cement, where as much as 1.9 wt.% Mo
303 (18900 ppm) was determined (Ryb et al. 2009) – the concentration rarely attainable even in rich Mo
304 ores. Molybdenum is disseminated among dispersed iron oxides, with no own mineral phases
305 resolvable at the level of conventional scanning electron microscope (our data). Besides the
306 abnormally high overall Mo content, ferriginous dolomite breccias are characterized by
307 unprecedented Mo isotopic variations ($\delta^{97/95}$Mo from –0.6 to +2.3 ‰) – the largest spread reported
308 in geological systems (Ryb et al. 2009). The origin of the breccias was explained by the influence of
309 hydrothermal solutions – the subsurface brines circulated in the sediments before the onset of the
310 Dead Sea rifting (Margaritz et al. 1983; Gilat 1994). It is noteworthy that the most significant Mo
311 anomaly is situated in the Zohar anticline, ~2 km away from the Hatrurim Basin (Ryb et al. 2009).
312 Although direct contacts between the sediments of the Bina and Menuha Formations and the
313 Mottled Zone were not observed (Fig. 3), one can suggest that Mo-rich dolomite breccias could be
314 entrapped and uplifted during pyrometamorphic processes. The upward transport of underlying
315 sediments through the clastic dykes and explosion pipes was reported in the Hatrurim Basin (Sokol
316 et al. 2007). The composition of ferriginous breccias is well suited for the pyrolytic transformation
317 into diopside rocks: dolomite and chert as the source of Ca, Mg and Si for diopside; hematite and

318 goethite as precursors for magnetite. An addition, the breccias are enriched in Ni, up to 1000 ppm
319 (Issar et al. 1969), while the source of phosphorus can be ascribed to the phosphorites of the
320 underlying Mishash Formation (Fig. 3). In the Jordan, the sediments of the Belqa group are the
321 obvious source of both Mo and Ni (Fleurance et al. 2013). As a consequence, one can suggest that
322 Mo-rich phosphide mineralization of the Mottled Zone is linked to the processes of polymetallic
323 enrichment of the sediments related to the development of the Dead Sea Transform fault system
324 (Ben-Avraham 2014). The subsequent formation of Mo-phosphides in pyrometamorphic rocks could
325 be accomplished *via* the co-reduction of phosphates and Mo- and Ni-bearing phases (powellite,
326 $CaMoO_4$, trevorite, $FeNi_2O_4$, bunsenite, NiO) with natural hydrocarbons or molecular dihydrogen,
327 as it was demonstrated on synthetic Mo-Ni-P systems (Burns et al. 2007).
328

329 **Mo and Ni as anthropogenic contaminants**

330 Zaccarini et al. (2019) recently described a mineral named tsikourasite, a Ni-Mo phosphide
331 found in the heavy mineral concentrate from chromitites of the Othrys ophiolite, Greece. This report
332 follows the growing number of articles on "super-reduced" or "ultra-reduced" mineral phases,
333 whose reliability was arguably doubted in the recent papers (Litasov et al. 2018, 2019; Ballhaus et
334 al. 2021). It appears symptomatic that the majority of these minerals, like those reported by
335 Zaccarini et al. (2019) or Xiong et al. (2020), come from mechanically ground probes taken from
336 chromitites of ophiolite complexes. Concerning the contents of our work, we have to give some
337 critical comments on the findings made by Zaccarini et al. (2019). It is noteworthy that
338 contamination of geological probes from grinding equipment is a well known problem (Butler et al.
339 2017). Molybdenum and nickel, being the constituents of heavy-duty superalloys (e.g., Darolia
340 2019), are proven contaminants of the probes prepared with the usage of mechanical grinders (e.g.,
341 Schmidt and Pearce 1981; Sertek et al. 2015). Besides superalloys as such, Ni-Mo and Ni-Co-Mo
342 compositions are used as the metal binders in diamond drilling tools (Loginov et al. 2019) and in the

so-called *cermets* – composite ceramic/metal materials prepared from superhard carbides or nitrides (WC, TiC, Mo_2C, TiN etc.) bound by the superalloy matrix. Cermets are commonly served as wear-resistant parts in grinders, milling and drilling equipment (Agnew et al. 2017; Ghasali et al. 2018; Panov 2020). In order to tighten the contacts between steel parts and superalloys, many types of brazing alloys (fillers) were introduced in industry. For the purposes of Ni-Mo alloys brazing, AWS BNi-6 composition is often used (American Welding Society 2007). Besides, this filler is used for brazing of diamond-based tools (Rabinkin et al. 2013). BNi-6 is a nickel-phosphorus eutectic containing 10-12 wt.% P and Ni by balance, that corresponds to the stoichiometry intermediate between Ni_5P and Ni_4P. An example of surficial contamination of the drill core with BNi-6 is given in Supplementary Fig. S1. It should be emphasized that BNi-6, while melted during brazing, is capable of selective extraction of Mo from Ni-Mo-Cr alloys, yielding Ni-Mo and Mo-phosphides (Jalilian et al. 2013). BNi-6 is not the only possible source of contamination with Mo-Ni phosphides. Protective Ni-P and Ni-Mo-P coatings prepared by electroless deposition are widely used in industry since the fifties of the XX century (Krishnan et al. 2006; Vargas et al. 2006). Because in both cases (brazing and coating) the whole system is phosphorus-deficient, the resultant phosphides are also phosphorus-deficient (M:P > 1).

Zaccarini et al. (2019) give no details on the grinding procedures they employed for the separation of phosphide grains. However, in the next article, the same authors indicate that the grinding equipment contained the parts made of some Mo-Cr superalloy, which they termed by the indefinable name “Alloy 1” (Bindi et al. 2020). Consequently, Zaccarini et al. (2019) used high-Mo superalloy during grinding procedures that would inevitably result in Mo contamination. That is, along with the low-phosphorus composition of tsikourasite, $Mo_3Ni_2P_{1+x}$ and associated phases, e.g., melliniite-like phosphide ~Ni_4P (= BNi-6), altogether with abnormally high Co contents, allows suggesting that phosphide assemblages described by Zaccarini et al. (2019) have anthropogenic origin. They likely represent the chunks of brazed Mo-superalloy joints, which were trapped by

chromite ore at the unknown stage of the grinding/separation process. The "intergrowths" between phosphide/metal and rock-forming minerals must not obfuscate the observer: the pressures attained in drilling/grinding operations are high enough for the alloy phases to be imprinted into (or spread over) the chromite or silicate grains (see Supplementary Fig. S1).

Implications

Polekhovskyite is a striking example of a new type of terrestrial Mo mineralization confined to phosphides of the Dead Sea Transform area. Mineral assemblages of this region are unique on Earth with regard to a diverse speciation of redox-sensitive elements. Further comparison of isotopic Mo ratios in phosphides and surrounding sediments (Ryb et al. 2009) would shed light on the likely sources of this element in the rocks of the Hatrurim Formation. The genesis of this world's largest pyrometamorphic complex, which encompasses an area of 150×200 km in the Middle East, remains enigmatic. The problem of the source of the incoming heat, which has led to the calcination and fusion of 200 m thick sedimentary sequence, is still unresolved. There is also no answer to the question whether the combustion of the carbon-bearing sediments was a spontaneous process or was it induced by some external event (Britvin et al. 2021b, 2022).

Yet another implication of the present work is a discussion of anthropogenic contamination of geological probes with Mo and Ni – a problem related to the use of superalloys in the mining industry and in the laboratory reprocessing of geological samples. This problem is exemplified by analysis of the origin of "ultra-reduced" phosphide assemblages reported from chromite concentrates (Zaccarini et al. 2019; Bindi et al. 2020). In this respect, our article complements the discussion opened by Litasov et al. (2018, 2019) and Ballhaus et al. (2021). Unfortunately, the manufacturers of grinding and drilling equipment avoid disclosing the compositions of superalloys, coatings or brazing fillers. As a consequence, obtaining this information relies upon a good will of mineralogists who are working with ore concentrates. The main problem here is that discrimination

between "atypical yet natural" and technogenic phases implies a deep involvement in the specific branches of materials science, outside of the areas covered by geosciences. Besides, tracking the sources of industrial contamination across the ore processing flowcharts implies high analytical costs, which may became comparable with the budgets of corresponding scientific projects. However, ignoring the prerequisites listed above may result in the lack of sufficient due diligence in revelation of anthropogenic factor. This tendency, quite typical of the "Anthropocene Epoch" (Hazen et al. 2017), may have long-lasting consequences: the niche currently occupied by the natural mantle minerals can be gradually superseded by a diverse collection of super-reduced anthropogenic phases.

Acknowledgments

The authors are indebted to the referees, Robert Hazen and Chris Ballhaus, for the linguistic support, helpful comments and suggestions, and to Fabrizio Nestola for editorial handling of the manuscript. This work was carried out with financial support of the Russian Science Foundation, grant 18-17-00079. The instrumental resources were provided by the Centre for X-ray Diffraction Studies and Geomodel Resource Center of Saint Petersburg State University.

References cited

Al-Tawalbeh, M., Atallah, M., and Al Tamimi, M. (2017). Structural evolution of the area north of Ajloun Dome, Jordan. Jordan Journal of Earth and Environmental Sciences, 8, 55–60.

Amelin, Y., Kaltenbach, A., Iizuka, T., Stirling, C.H., Ireland, T.R., Petaev, M. and Jacobsen, S.B. (2010) U–Pb chronology of the Solar System's oldest solids with variable $^{238}U/^{235}U$. Earth and Planetary Science Letters, 300, 343–350.

Agnew, S.R., Keene, J.I., Dong, L., Shamsujjoha, M., O'Masta, M.R., and Wadley, H.N.G. (2017) Microstructure characterization of large TiC-Mo-Ni cermet tiles. International Journal of Refractory Metals and Hard Materials, 68, 84–95.

American Welding Society. Brazing handbook. 5th ed. Miami (FL): American Welding Society; 2007.

Armstrong, T., Hutcheon, I.D., and Wasserburg, G.J. (1987) Zelda and company: petrogenesis of sulfide-rich Fremdlinge and constraints on solar nebula processes. Geochimica et Cosmochimica Acta, 51, 3155–3173.

Ballhaus, C., Helmy, H.M., Fonseca, R.O.C., Wirth, R., Schreiber, A., and Jöns, N. (2021) Ultra-reduced phases in ophiolites cannot come from Earth's mantle. American Mineralogist, 106, 1053–1063.

Ben-Avraham, Z., Garfunkel, Z., and Lazar, M. (2008) Geology and evolution of the Southern Dead Sea Fault with emphasis on subsurface structure. Annual Review of Earth and Planetary Sciences, 36, 357–387.

Ben-Avraham, Z. (2014) Geophysical studies of the crustal structure along the southern Dead Sea Fault. In Z. Garfunkel, Z. Ben-Avraham, E. Kagan, Ed., Dead Sea Transform Fault System: Reviews, p. 1–28. Springer, Netherlands.

Bindi, L., Zaccarini, F., Ifandi, E., Tsikouras, B., Stanley, C., Garuti, G., and Mauro, D. (2020) Grammatikopoulosite, NiVP, a new phosphide from the chromitite of the Othrys ophiolite, Greece. Minerals, 10, 131.

Bogoch, R., Gilat, A., Yoffe, O., and Ehrlich, S. (1999). Rare earth trace element distributions in the Mottled Zone complex, Israel. Israel Journal of Earth Sciences, 48, 225–234.

Britvin, S.N., Murashko, M.N., Vapnik, Ye., Polekhovsky, Yu.S., and Krivovichev, S.V. (2015) Earth's phosphides in Levant and insights into the source of Archaean prebiotc phosphorus. Scientific Reports, 5, 8355.

441 Britvin, S.N., Murashko, M.N., Vapnik, Ye., Polekhovsky, Yu.S., Krivovichev, S.V., Vereshchagin,
442 O.S., Vlasenko, N.S., Shilovskikh, V.V., and Zaitsev, A.N. (2019a) Zuktamrurite, FeP_2, a new
443 mineral, the phosphide analogue of löllingite, $FeAs_2$. Physics and Chemistry of Minerals, 46,
444 361–369.
445 Britvin, S.N., Vapnik, Ye., Polekhovsky, Yu.S. and Krivovichev, S.V., Krzhizhanovkaya M.G.,
446 Gorelova, L.A., Vereshchagin, O.S., Shilovskikh, V.V., and Zaitsev, A.N. (2019b)
447 Murashkoite, FeP, a new terrestrial phosphide from pyrometamorphic rocks of the Hatrurim
448 Formation, Southern Levant. Mineralogy and Petrology, 113, 237–248.
449 Britvin, S.N., Murashko, M.N., Vapnik, Y., Zaitsev, A.N., Shilovskikh, V.V., Vasiliev, E.A.,
450 Krzhizhanovskaya, M.G., and Vlasenko, N.S. (2019c) IMA 2019-039. CNMNC Newsletter
451 No. 51; Mineralogical Magazine, 83, 759.
452 Britvin, S.N., Murashko, M.N., Vapnik, Ye., Polekhovsky, Yu.S., Krivovichev, S.V.,
453 Krzhizhanovskaya, M.G., Vereshchagin, O.S., Shilovskikh, V.V., and Vlasenko, N.S. (2020a)
454 Transjordanite, Ni_2P, a new terrestrial and meteoritic phosphide, and natural solid solutions
455 barringerite–transjordanite (hexagonal Fe_2P–Ni_2P). American Mineralogist, 105, 428–436.
456 Britvin, S.N., Murashko, M.N., Vapnik, Ye., Polekhovsky, Yu.S., Krivovichev, S.V., Vereshchagin,
457 O.S., Shilovskikh, V.V., Vlasenko, N.S., and Krzhizhanovskaya, M.G. (2020b) Halamishite,
458 Ni_5P_4, a new terrestrial phosphide in the Ni–P system. Physics and Chemistry of Minerals,
459 2020, 3.
460 Britvin, S.N., Murashko, M.N., Vapnik, Ye., Polekhovsky, Yu.S., Krivovichev, S.V., Vereshchagin,
461 O.S., Shilovskikh, V.V., and Krzhizhanovskaya, M.G. (2020c) Negevite, the pyrite-type NiP_2,
462 a new terrestrial phosphide. American Mineralogist, 105, 422–427.
463 Britvin, S.N., Murashko, M.N., Vapnik ,Ye., Vlasenko, N.S., Krzhizhanovskaya, M.G.,
464 Vereshchagin, O.S., Bocharov, V.N., and Lozhkin, M.S. (2021a) Cyclophosphates, a new class

of native phosphorus compounds, and some insights into prebiotic phosphorylation on early Earth. Geology, 49, 382–386.

Britvin, S.N., Vereshchagin, O.S., Shilovskikh, V.V., Krzhizhanovskaya, M.G., Gorelova, L.A., Vlasenko, N.S., Pakhomova, A.S., Zaitsev, A.N., Zolotarev, A.A., Bykov, M., Lozhkin, M.S., and Nestola, F. (2021b) Discovery of terrestrial allabogdanite $(Fe,Ni)_2P$, and the effect of Ni and Mo substitution on the barringerite-allabogdanite high-pressure transition. American Mineralogist, 106, 944–952.

Britvin, S.N., Krzhizhanovskaya, M.G., Zolotarev, A.A., Gorelova, L.A., Obolonskaya, E.V., Vlasenko, N.S., Shilovskikh, V.V., and Murashko, M.N. (2021c) Crystal chemistry of schreibersite, $(Fe,Ni)_3P$. American Mineralogist, 106, 1520–1533.

Britvin, S.N., Galuskina, I.O., Vlasenko, N.S., Vereshchagin, O.S., Bocharov, V.N., Krzhizhanovskaya, M.G., Shilovskikh, V.V., Galuskin, E.V., Vapnik, Ye.V., and Obolonskaya, E.V. (2021d) Keplerite, $Ca_9(Ca_{0.5}\square_{0.5})Mg(PO_4)_7$, a new meteoritic and terrestrial phosphate isomorphous with merrillite, $Ca_9NaMg(PO_4)_7$. American Mineralogist, 106, DOI 10.2138/am-2021-7834

Britvin, S.N., Vlasenko, N.S., Aslandukov, A., Aslandukova, A., Dubrovinsky, L., Gorelova, L.A., Krzhizhanovskaya, M.G., Vereshchagin, O.S., Bocharov, V.N., Shelukhina, Yu.S., Lozhkin, M.S., Zaitsev, A.N., and Nestola, F. (2022) Natural cubic perovskite, $Ca(Ti,Si,Cr)O_{3-\delta}$, a versatile potential host for rock-forming and less-common elements up to Earth's mantle pressure. American Mineralogist, DOI 10.2138/am-2022-8186

Burg, A., Starinsky. A., Bartov. Y., and Kolodny, Y. (1992) Geology of the Hatrurim Formation ("Mottled Zone") in the Hatrurim basin. Israel Journal of Earth Sciences, 40, 107–124.

Burns, S., Hargreaves, J.S.J., and Hunter, S.M. (2007) On the use of methane as a reductant in the synthesis of transition metal phosphides. Catalysis Communications, 8, 931–935.

Butler, O.T., Cairns, W.R.L., Cook, J.M., and Davidson, C.M. (2017) Atomic spectrometry update - a review of advances in environmental analysis. Journal of Analytical Atomic Spectrometry, 32, 11–57.

Darolia, R. (2019) Development of strong, oxidation and corrosion resistant nickel-based superalloys: critical review of challenges, progress and prospects. International Materials Reviews, 64, 355–380.

Dolomanov, O.V., Bourhis, L.J., Gildea, R.J., Howard, J.A., and Puschmann, H. (2009) OLEX2: a complete structure solution, refinement and analysis program. Journal of Applied Crystallography, 42, 339–341.

Dowty, E. (2006). ATOMS for Windows. Shape Software, Kingsport, Tennessee, USA.

El Goresy, A., Nagel, K., and Ramdohr, P. (1978) Fremdlinge and their noble relatives. Proceedings of the Lunar and Planetary Science Conference, 9, 1279–1303.

Erickson, B.E., and Helz, G.R. (2000) Molybdenum(VI) speciation in sulfidic waters: stability and lability of thiomolybdates. Geochimica et Cosmochimica Acta, 64, 1149–1158.

Fleurance, S., Cuney, M., Malartre, M., and Reyx, J. (2013) Origin of the extreme polymetallic enrichment (Cd, Cr, Mo, Ni, U, V, Zn) of the Late Cretaceous–Early Tertiary Belqa Group, central Jordan. Palaeogeography, Palaeoclimatology, Palaeoecology, 369, 201–219.

Fuchs, L.H., and Blander, M. (1977) Molybdenite in calcium-aluminium-rich inclusions in the Allende meteorite. Geochimica et Cosmochimica Acta, 41, 1170–1174.

Galuskin, E., Galuskina, I., Vapnik, Ye., and Murashko, M. (2020) Molecular hydrogen in natural mayenite. Minerals, 10, 560.

Galuskina, I.O., Galuskin, E.V., Prusik, K., Vapnik, Y., Juroszek, R., Jeżak, L., and Murashko, M. (2017) Dzierżanowskite, $CaCu_2S_2$ – a new natural thiocuprate from Jabel Harmun, Judean Desert, Palestine Autonomy, Israel. Mineralogical Magazine, 81, 1073–1085.

513 Geller, Y.I., Burg, A., Halicz, L., and Kolodny, Y. (2012) System closure during the combustion
514 metamorphic "Mottled Zone" event, Israel. Chemical Geology, 334, 25–36.
515 Ghasali, E., Ebadzadeh, T., Alizadeh, M., and Razavi, M. (2018) Mechanical and microstructural
516 properties of WC-based cermets: A comparative study on the effect of Ni and Mo binder
517 phases. Ceramics International, 44, 2283–2291.
518 Gilat, A. (1994) Tectonic and associated mineralization activity, Southern Judea, Israel. Geological
519 Survey of Israel, Report GSI/19/94, Jerusalem, 322 p.
520 Greaney, A.T., Rudnick, R.L., Gaschnig, R.M., Whalen, J.B., Luais, B., and Clemens, J.D. (2018)
521 Geochemistry of molybdenum in the continental crust. Geochimica et Cosmochimica Acta,
522 238, 36–54.
523 Gross, S. (1977) The mineralogy of the Hatrurim Formation, Israel. Geological Survey of Israel
524 Bulletin, 70, 1–80.
525 Guérin, R. (1976) Nouveaux arséniures et phosphures ternaires de molybdène ou de tungstène et
526 d'éléments 3d, à chaînes métal – métal: Structures et Propriétés. PhD Thesis, Univerity of
527 Rennes, 263 p.
528 Guérin, R., Sergent, M., and Chaudron, G. (1975) Synthese et étude radiocristallographique des
529 systemes MP − MoP et MP − WP (M = element 3d). Comptes Rendus des Academie Sciences
530 Serie C, 281, 777–780.
531 Guérin, R., and Sergent, M. (1976) Nouveau phosphure ternaire: $NiMoP_2$, a chaine linéaire infinite –
532 Mo–Ni–Mo– et composés isotypes: $NiWP_2$, $CoMoP_2$ et $CoWP_2$. Journal of Solid State
533 Chemistry, 18, 317–323.
534 Guérin, R., and Sergent, M. (1977) Nouveaux arseniures et phosphures ternaires de molybdene ou
535 de tungstene et d'elements 3d, de formule: $M_{2-x}Me_xX$ (M = élément 3d; Me = Mo, W; X = As,
536 P). Materials Research Bulletin, 12, 381–388.

537 Gur, D., Steinitz, G., Kolodny, Y., Starinsky, A., and McWilliams, M. (1995) $^{40}Ar/^{39}Ar$ dating of
538 combustion metamorphism ("Mottled Zone", Israel). Chemical Geology, 122, 171–184.
539 Hazen, R.M., Grew, E.S., Origlieri, M., and Downs, R.T. (2017) On the mineralogy of the
540 "Anthropocene Epoch". American Mineralogist, 102, 595–611.
541 Ilani, S., Kronfeld, J., and Flexer, A. (1985) Iron-rich veins related to structural lineaments, and the
542 search for base metals in Israel. Journal of Geochemical Exploration, 24, 197–206.
543 Issar, A., Eckstein, Y., and Bogoch, R. (1969) A possible thermal spring deposit in the Arad area,
544 Israel. Israel Journal of Earth Sciences, 18, 17–20.
545 Jalilian, F., Jahazi, M., and Drew, R.A.L. (2013) Microstructure Evolution During Transient Liquid
546 Phase Bonding of Alloy 617. Metallography, Microstructure, and Analysis, 2, 170–182.
547 Juroszek, R., Krüger, B., Galuskina, I., Krüger, H., Vapnik, Y., and Galuskin, E. (2020) Siwaqaite,
548 $Ca_6Al_2(CrO_4)_3(OH)_{12}\cdot 26H_2O$, a new mineral of the ettringite group from the pyrometamorphic
549 Daba-Siwaqa complex, Jordan. American Mineralogist, 105, 409–421.
550 Kendall, B., Dahl, T.W., and Anbar, A.D. (2017). The stable isotope geochemistry of molybdenum.
551 Reviews in Mineralogy and Geochemistry, 82, 683–732.
552 Khoury, H. N. (2020) High- and low-temperature mineral phases from the pyrometamorphic rocks,
553 Jordan. Arabian Journal of Geosciences, 13, 734.
554 Krishnan, K.H., John, S., Srinivasan, K., Praveen, J., Ganesan, M., and Kavimani, P. (2006) An
555 overall aspect of electroless Ni-P depositions - a review article. Metallurgical and Materials
556 Transactions A, 37, 1917–1926.
557 Lazoryak, B.I., Belik, A.A., Kotov, R.N., Leonidov, I.A., Mitberg, E.B., Karelina, V.V., Kellerman,
558 D.G., Stefanovich, S.Y., and Avetisov, A.K. (2003) Reduction and re-oxidation behavior of
559 calcium iron phosphate, $Ca_9Fe(PO_4)_7$. Chemistry of Materials, 15, 625–631.

560 Litasov, K.G., Kagi, H., and Bekker, T.B. (2018) Enigmatic super-reduced phases in corundum from
561 natural rocks: Possible contamination from artificial abrasive materials or metallurgical slags.
562 Lithos, 340, 181–190.
563 Litasov, K.G., Kagi, H., Voropaev, S.A., Hirata, T., Ohfuji, H., and Ishibashi, H. (2019) Comparison
564 of enigmatic diamonds from the Tolbachik arc volcano (Kamchatka) and Tibetan ophiolites:
565 Assessing the role of contamination by synthetic materials. Gondwana Research, 75, 16–27.
566 Loginov, P.A., Sidorenko, D.A., Bychkova, M.Y., Zaitsev, A.A., and Levashov, E.A. (2019)
567 Performance of diamond drill bits with hybrid nanoreinforced Fe-Ni-Mo binder. The
568 International Journal of Advanced Manufacturing Technology, 102, 2041–2047.
569 Ma, C., Beckett, J.R., and Rossman, G.R. (2014) Monipite, MoNiP, a new phosphide mineral in a
570 Ca-Al-rich inclusion from the Allende meteorite. American Mineralogist, 99, 198–205.
571 Magaritz, M., Issar, A., and Azmon, E. (1983) On the genesis of discordant dolostone bodies in the
572 northeastern Negev, Israel. Chemical Geology, 39, 93–114.
573 Murashko, M.N., Vapnik, Ye., Polekhovsky, Y.P., Shilovskikh, V.V., Zaitsev, A.M., Vereshchagin,
574 O.S., and Britvin, S.N. (2019) Nickolayite, IMA 2018-126. CNMNC Newsletter No. 47.
575 Mineralogical Magazine, 83, 146.
576 Nathan, Y., Shiloni, Y., Roded, R., Gal, I., and Deutsch, Y. (1979) The geochemistry of the northern
577 Negev phosphorites (Southern Israel). Geological Survey of Israel, Bulletin, 73, 41 p.
578 Novikov, I., Vapnik, Ye., and Safonova, I. (2013) Mud volcano origin of the Mottled Zone,
579 Southern Levant. Geoscience Frontiers, 4, 597–619.
580 Oryshchyn, S.V., Le Sénéchal, C., Députier, S., Bauer, J., Guérin, R., and Akselrud, L.G. (2001)
581 New ternary phases in the Mo-Ni-P system: Synthesis and crystal structures. Journal of Solid
582 State Chemistry, 160, 156–166.
583 Panov V.S. (2020) Tungsten-free hard alloys: an analytical review. Inorganic Materials: Applied
584 Research, 11, 823–829.

585 Pasek, M., and Block, K. (2009) Lightning-induced reduction of phosphorus oxidation state. Nature
586 Geoscience, 2, 553–556.
587 Pekov, I.V., Zubkova, N.V., Koshlyakova, N.N., Belakovskiy, D.I., Agakhanov, A.A., Vigasina,
588 M.F., Britvin, S.N., Sidorov, E.G., and Pushcharovsky, D.Yu. (2020) Rhabdoborite-(V),
589 rhabdoborite-(Mo) and rhabdoborite-(W): a new group of borate minerals with the general
590 formula $Mg_{12}M_{11/3}O_6$ $[(BO_3)_{6-x}(PO_4)_xF_{2-x}]$ ($M = V^{5+}$, Mo^{6+} or W^{6+} and $x < 1$). Physics and
591 Chemistry of Minerals, 47, 44.
592 Picard, L. Geological researches in the Judean Desert. Jerusalem, Goldberg Press, 1931, 108 p.
593 Rabinkin, A., Shapiro, A.E., and Boretius, M. (2013) Brazing of diamonds and cubic boron nitride.
594 in: Advances in Brazing: Science, Technology and Applications, Woodhead Publishing,
595 Cambridge, 160–193.
596 Ryb, U., Erel, Y., Matthews, A., Avni, Y., Gordon, G.W., and Anbar, A.D. (2009) Large
597 molybdenum isotope variations trace subsurface fluid migration along the Dead Sea transform.
598 Geology, 37, 463–466.
599 Schmidt, P.F., Pearce, C.W. (1981) A neutron activation analysis study of the sources of transition
600 group metal contamination in the silicon device manufacturing process. Journal of The
601 Electrochemical Society, 128, 630–637.
602 Sertek, J.P., Andrade, S., and Ulbrich, H.H. (2015) An evaluation of the effects of primary and
603 cross-contamination during the preparation of rock Powders for chemical determinations.
604 Geostandards and Geoanalytical Research, 39, 381–397.
605 Sharygin, V.V., Vapnik, Y., Sokol, E.V., Kamenetsky, V.S., and Shagam, R. (2016) Melt inclusions
606 in minerals of schorlomite-rich veins of the Hatrurim Basin, Israel: Composition and
607 homogenization temperatures. In P. Ni, Z. Li, Eds., Proceedings of the ACROFI I, p. 189–192,
608 Elsevier, The Netherlands.

609 Smith, J. (1971) The truth of rocks in Florida. In B. Jones and C. Doe, Eds., Proceedings of the third
610 conference on Florida rocks, p. 224-228. Mineralogical Society of Florida, Miami.
611 Sheldrick, G.M. (2015) Crystal structure refinement with *SHELXL*. Acta Crystallographica, C71, 3–
612 8.
613 Smedley, P.L., and Kinniburgh, D.G. (2017) Molybdenum in natural waters: A review of
614 occurrence, distributions and controls. Applied Geochemistry, 84, 387–432.
615 Sokol, E.V., Novikov, I.S., Vapnik, Ye., and Sharygin, V.V. (2007) Gas fire from mud volcanoes as
616 a trigger for the appearance of high-temperature pyrometamorphic rocks of the Hatrurim
617 Formation (Dead Sea area). Doklady Earth Sciences, 413A, 474–480 (in Russian).
618 Sokol, E.V., Kokh, S.N., Seryotkin, Yu.V., Deviatiiarova, A.S., Goryainov, S.V., Sharygin, V.V.,
619 Khoury, H.N., Karmanov, N.S., Danilovsky, V.A., and Artemyev, D.A. (2020) Ultrahigh-
620 temperature sphalerite from Zn-Cd-Se-rich combustion metamorphic marbles, Daba complex,
621 Central Jordan: Paragenesis, Chemistry, and Structure. Minerals, 10, 822.
622 Vapnik, Ye., Sharygin, V.V., Sokol, E.V., and Shagam, R. (2007) Paralavas in a combustion
623 metamorphic complex: Hatrurim Basin, Israel. The Geological Society of America, Reviews in
624 Engineering Geology, 18, 133–153.
625 Vapnik, Y., Galuskina, I., Palchik, V., Sokol, E.V., Galuskin, E., Lindsley-Griffin, N., and Stracher,
626 G.B. (2015) Stone-tool workshops of the Hatrurim Basin, Israel. In G.B. Stracher, A. Prakash
627 and E.V. Sokol, Eds., Coal and Peat Fires: A Global Perspective 3, p. 281–316, Elsevier, The
628 Netherlands.
629 Vargas, L., Barba, A., Sánchez, F., and Bolarín, A. (2006) Age hardening of Ni-P-Mo electroless
630 deposit. Surface Engineering, 22, 58–62.
631 Voncken, H.L., Scheepers, E., and Yang, Y. (2006) Analysis of uranium-bearing Fe-phosphide grain
632 from a submerged arc furnace for phosphorus production. Mineralogy and Petrology, 88, 407–
633 418.

634 Xiong, F., Xu, X., Mugnaioli, E., Gemmi, M., Wirth, R., Grew, E.S., Robinson, P.T., and Yang, J.
635 (2020) Two new minerals, badengzhuite, TiP, and zhiqinite, $TiSi_2$, from the Cr-11 chromitite
636 orebody, Luobusa ophiolite, Tibet, China: is this evidence for super-reduced mantle-derived
637 fluids? European Journal of Mineralogy, 32, 557–574.
638 Zaccarini, F., Bindi, L., Ifandi, E., Grammatikopoulos, T., Stanley, C., Garuti, G., and Mauro, D.
639 (2019) Tsikourasite, $Mo_3Ni_2P_{1+x}$ ($x < 0.25$), a new phosphide from the chromitite of the Othrys
640 ophiolite, Greece. Minerals, 9, 248.
641

642 **List of figure captions**

643

644 **Figure 1.** An overview map of the southern Levant. The small Mottled Zone outcrops are marked
645 with red circles. The Hatrurim Basin and Daba-Siwaqa complex are shown as outlined areas.
646 Modified from Britvin et al. 2021a (CC-BY).

647

648 **Figure 2.** Phosphide localities and phosphide-bearing lithologies of the Mottled Zone. (a) Wadi
649 Halamish in the Hatrurim Basin, Israel – a type locality for a variety of phosphides, including
650 polekhovskyite. Adapted from Britvin et al. (2015) (CC-BY). (b) A piece of hydrothermally altered
651 diopside microbreccia from wadi Halamish – the rock host for phosphide assemblages. Dark areas
652 are coloured with hematite and magnetite. The patches of olive color indicate secondary phosphate
653 mineralization. (c) A 2×2 m outcrop of phosphide-bearing rocks at wadi Zohar, Hatrurim Basin,
654 described in Galuskin et al. (2020). (d) Polished plate of a fused gehlenite rock containing
655 phosphides, wadi Zohar. (e) A block of pyrometamorphic rock where the dark areas bear phosphide
656 mineralization. Phosphorite quarry at the Daba-Siwaqa complex, west Jordan. (f) Polished plate of
657 brecciated phosphide-bearing paralava from this phosphorite quarry. The black areas trace the
658 inclusions of phosphide minerals.

659

660 **Figure 3.** Stratigraphic position of the Hatrurim Basin, Israel, and Daba-Siwaqa complex, Jordan, in
661 the Late Cretaceous–Paleogene sequence of the southern Levant. The stratigraphic equivalents of
662 the Mottled Zone are highlighted by color. Drawn based on the data of Gross 1977, Novikov et al.
663 2013, and Al-Tawalbeh et al. 2017.

664

665 **Figure 4.** A centimeter-sized phosphide nest (resembling sulfides) in the diopside rock. Phosphorite quarry at
666 the Daba-Siwaqa complex, West Jordan (cf. Fig. 2e, 2f).

667 **Figure 5.** Polekhovskyite crystals in phosphide assemblage within the altered diopside paralava. (a)
668 SEM BSE image. (b) The same area in reflected light, after removal of carbon coating. Wadi
669 Halamish, Hatrurim Basin, Israel. Abbreviations: Pkh – polekhovskyite; Muh – murashkoite; Tjrd –
670 transjordanite; Ap – fluorapatite.
671
672 **Figure 6.** Crystal structures of (a) polekhovskyite, $MoNiP_2$, and (b) synthetic analogue of monipite,
673 MoNiP. In the structure of polehovskyite, face-sharing $[NiP_6]$ octahedra (green) and $[MoP_6]$ trigonal
674 prisms (red) alternate along the *c*-axis. In MoNiP, perforated layers of corner-sharing $[NiP_4]$
675 tetrahedra (green) alternate with perforated layers of corner- and edge-sharing $[MoP_5]$ square prisms
676 (red). Drawn in ATOMS v.6 (Dowty 2006).
677
678 **Figure 7.** Non-phosphide Mo minerals in pyrometamorphic rocks of the Mottled Zone. (a)
679 Molybdenite (exsolution?) lamellae in a grain of murashkoite, FeP. (b) Molybdenite lamella in
680 zuktamrurite, FeP_2. (c) Euhedral grains of powellite, $CaMoO_4$, in association with magnetite,
681 aragonite and keplerite, $Ca_9(Ca_{0.5}\square_{0.5})Mg(PO_4)_7$ (Britvin et al. 2021d). SEM BSE images. Localities:
682 (a,c) Halamish wadi, Hatrurim basin, Negev desert, Israel. (b) Phosphorite quarry, Daba-Siwaqa
683 complex, Transjordan Plateau, Jordan. Abbreviations: Mol – molybdenite, Muh – murashkoite, Zuk
684 – zuktamrurite, Pwl – powellite, Arg – aragonite, Kep – keplerite.
685
686 **Figure 8.** (a) An outcrop of ferriginous dolomite breccia at the northern part of the Zohar anticline,
687 Negev desert, Israel (ca. 2 km away from the Hatrurim Basin). (b) A piece of the breccia composed
688 of dolomite fragments cemented with Mo-bearing goethite.
689
690
691

692 **Tables**

693
694
695 Table 1. Chemical composition (wt. %) of polekhovskyite and associated phosphides.
696

	Polekhovskyite *n* = 4 (range)	Murashkoite	Transjordanite
Mo	44.10 (43.78–44.34)	< 0.2	1.36
Ni	22.73 (22.55–22.96)	18.84	70.31
Fe	4.60 (4.52–4.66)	45.72	7.20
Co	< 0.2	< 0.2	< 0.2
P	29.02 (28.84–29.13)	35.63	21.24
Total	100.45	100.19	100.11
	Formula amounts		
	Σ = 4 *apfu*	Σ = 2 *apfu*	Σ = 3 *apfu*
Mo	0.99		0.02
Ni	0.83	0.28	1.77
Fe	0.18	0.72	0.19
P	2.01	1.00	1.02

697
698

This is the peer-reviewed, final accepted version for American Mineralogist, published by the Mineralogical Society of America.
The published version is subject to change. Cite as Authors (Year) Title. American Mineralogist, in press.
DOI: https://doi.org/10.2138/am-2022-8261. http://www.minsocam.org/

Table 2. Calculated powder X-ray diffraction pattern for polekhovskite (*d* in Å) in comparison with the reference pattern of synthetic $MoNiP_2$.

Polekhovskite [a]		$MoNiP_2$ [b]		
I_{calc}	d_{calc}	I_{meas}	d_{meas}	*hkl*
4	5.614	10	5.610	002
71	2.884	80	2.880	100
14	2.807	40	2.796	004
9	2.793			101
8	2.565	25	2.562	102
8	2.284	15	2.285	103
100	2.011	100	2.012	104
1	1.871	3	1.870	006
1	1.772	2	1.773	105
35	1.665	80	1.665	110
1	1.596	5	1.596	112
1	1.570	3	1.569	106
7	1.442	13	1.442	200
9	1.432	20	1.432	114
1	1.430			201
6	1.403	17	1.403	008
2	1.402			107
1	1.397			202
1	1.346			203

[a] This work; calculated for Cu*K*α-radiation on the basis of structural data, using Atoms v.6 (Dowty 2006). [b] Experimental pattern of synthetic $MoNiP_2$, Cu*K*α-radiation (Guérin 1976).

This is the peer-reviewed, final accepted version for American Mineralogist, published by the Mineralogical Society of America.
The published version is subject to change. Cite as Authors (Year) Title. American Mineralogist, in press.
DOI: https://doi.org/10.2138/am-2022-8261. http://www.minsocam.org/

Table 3. Crystal parameters of polekhovskyite, synthetic $MoNiP_2$ and MoNiP.

	Ideal formula	Structure type	Space group	a (Å)	c (Å)	V (Å^3)	Z
Polekhovskyite [1] [a]	$MoNiP_2$	$MoNiP_2$	$P6_3/mmc$	3.330(1)	11.227(4)	107.8(8)	2
Synthetic [2]	$MoNiP_2$	$MoNiP_2$	$P6_3/mmc$	3.329(3)	11.22(1)	107.7	2
Synthetic [3]	MoNiP	Fe_2P	$P\bar{6}2m$	5.861	3.704	110.2	3

[a] References: [1] This work; [2] Guérin and Sergent (1976); [3] Guérin and Sergent (1977).

This is the peer-reviewed, final accepted version for American Mineralogist, published by the Mineralogical Society of America.
The published version is subject to change. Cite as Authors (Year) Title. American Mineralogist, in press.
DOI: https://doi.org/10.2138/am-2022-8261. http://www.minsocam.org/

723 **Figures**

724

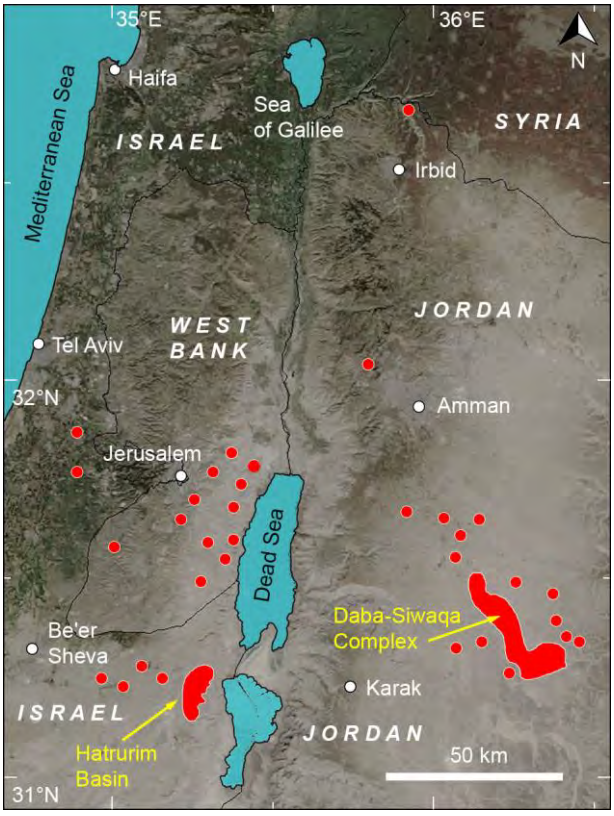

725

726

727 **Figure 1**

728

729

This is the peer-reviewed, final accepted version for American Mineralogist, published by the Mineralogical Society of America.
The published version is subject to change. Cite as Authors (Year) Title. American Mineralogist, in press.
DOI: https://doi.org/10.2138/am-2022-8261. http://www.minsocam.org/

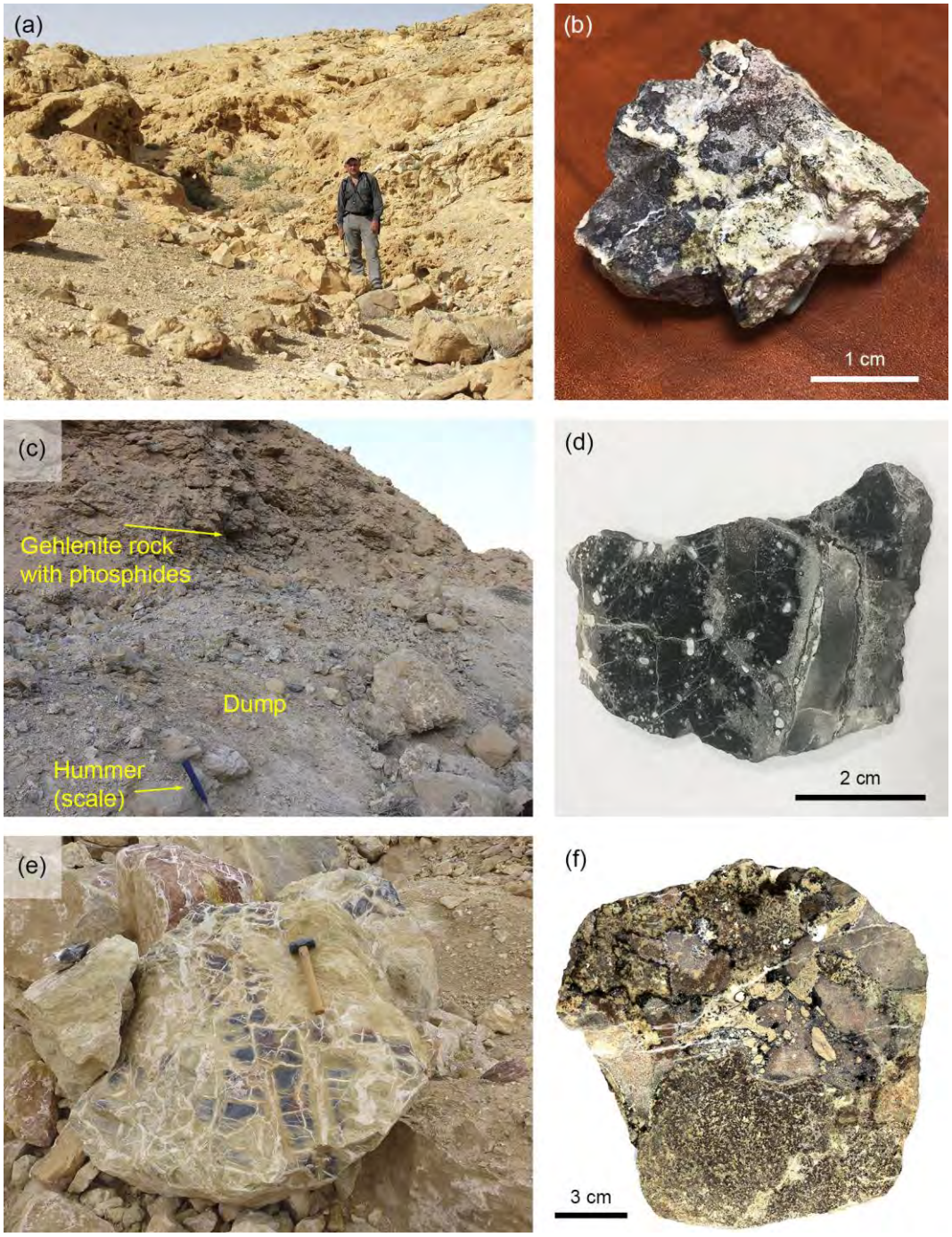

730

731

732 **Figure 2**

733

This is the peer-reviewed, final accepted version for American Mineralogist, published by the Mineralogical Society of America.
The published version is subject to change. Cite as Authors (Year) Title. American Mineralogist, in press.
DOI: https://doi.org/10.2138/am-2022-8261. http://www.minsocam.org/

734

735

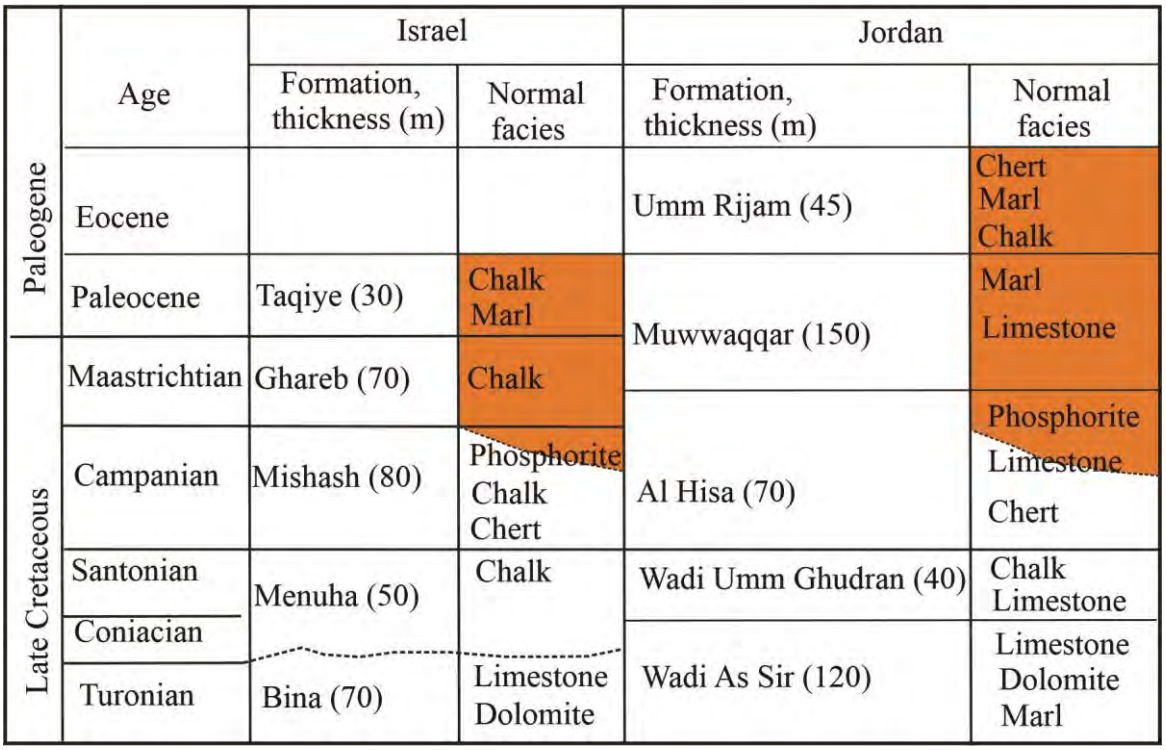

736

737

738 **Figure 3**

739

This is the peer-reviewed, final accepted version for American Mineralogist, published by the Mineralogical Society of America.
The published version is subject to change. Cite as Authors (Year) Title. American Mineralogist, in press.
DOI: https://doi.org/10.2138/am-2022-8261. http://www.minsocam.org/

740

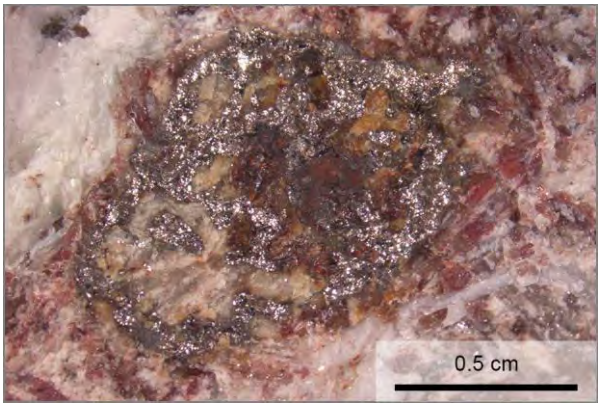

741

742

743 **Figure 4**

744

745

This is the peer-reviewed, final accepted version for American Mineralogist, published by the Mineralogical Society of America.
The published version is subject to change. Cite as Authors (Year) Title. American Mineralogist, in press.
DOI: https://doi.org/10.2138/am-2022-8261. http://www.minsocam.org/

746

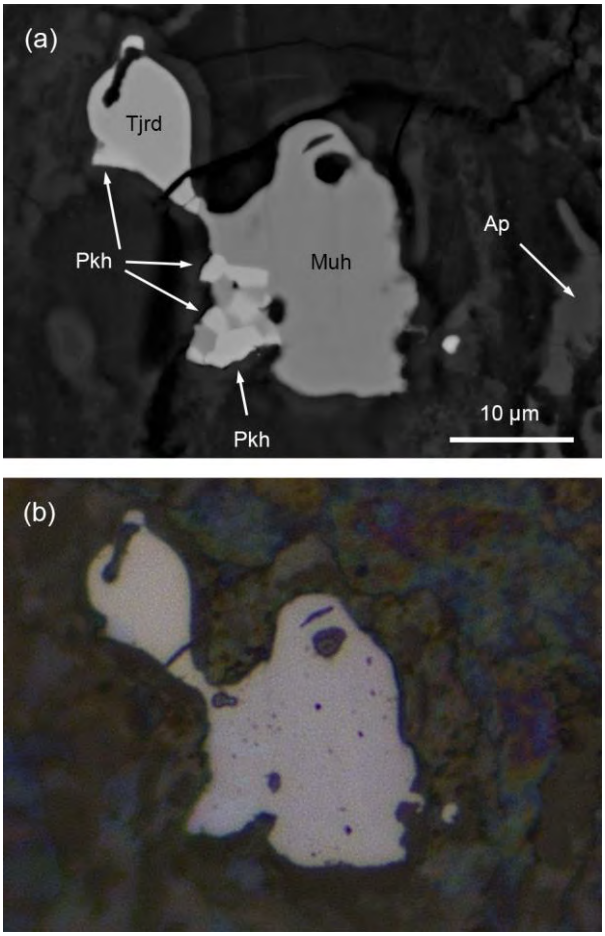

747

748

749 **Figure 5**

750

This is the peer-reviewed, final accepted version for American Mineralogist, published by the Mineralogical Society of America.
The published version is subject to change. Cite as Authors (Year) Title. American Mineralogist, in press.
DOI: https://doi.org/10.2138/am-2022-8261. http://www.minsocam.org/

751

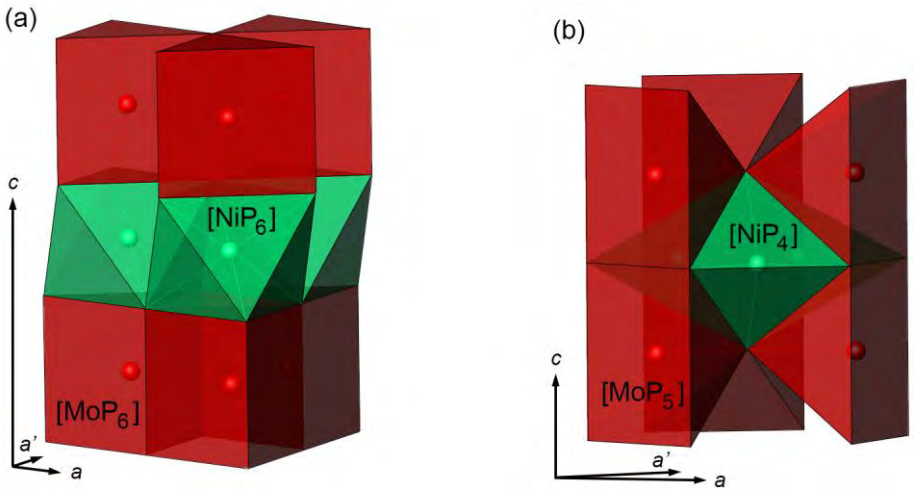

752

753

754 **Figure 6**

755

This is the peer-reviewed, final accepted version for American Mineralogist, published by the Mineralogical Society of America.
The published version is subject to change. Cite as Authors (Year) Title. American Mineralogist, in press.
DOI: https://doi.org/10.2138/am-2022-8261. http://www.minsocam.org/

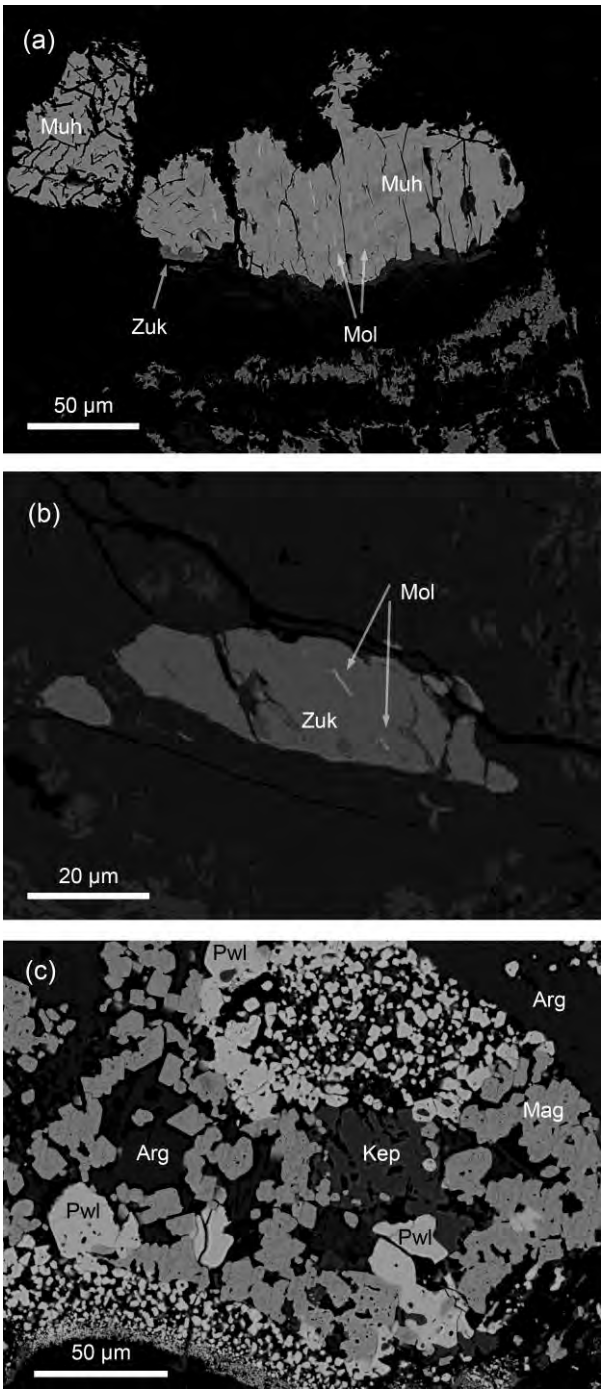

Figure 7

This is the peer-reviewed, final accepted version for American Mineralogist, published by the Mineralogical Society of America.
The published version is subject to change. Cite as Authors (Year) Title. American Mineralogist, in press.
DOI: https://doi.org/10.2138/am-2022-8261. http://www.minsocam.org/

761

762

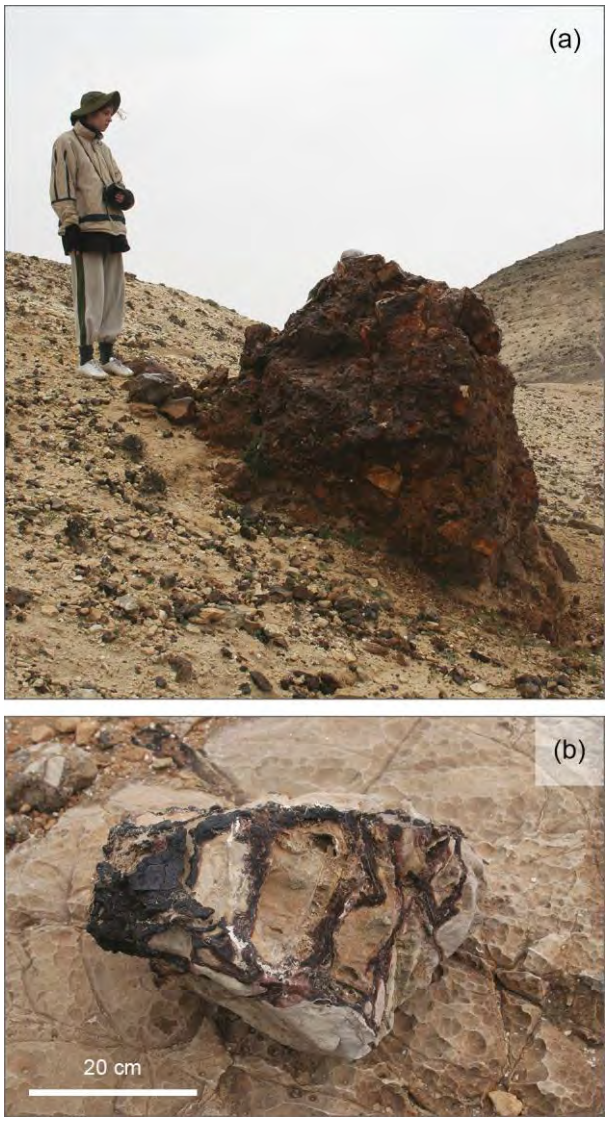

763

764

765 **Figure 8**